Eur J Nucl Med Mol Imaging (2015) 42:1707–1717
DOI 10.1007/s00259-015-3092-8

ORIGINAL ARTICLE

PET imaging of DNA damage using ^{89}Zr-labelled anti-γH2AX-TAT immunoconjugates

James C. Knight[1] · Caitríona Topping[1] · Michael Mosley[1] · Veerle Kersemans[1] · Nadia Falzone[1,2] · José M. Fernández-Varea[3] · Bart Cornelissen[1]

Received: 8 January 2015 / Accepted: 19 May 2015 / Published online: 2 June 2015

Abstract
Purpose The efficacy of most anticancer treatments, including radiotherapy, depends on an ability to cause DNA double-strand breaks (DSBs). Very early during the DNA damage signalling process, the histone isoform H2AX is phosphorylated to form γH2AX. With the aim of positron emission tomography (PET) imaging of DSBs, we synthesized a ^{89}Zr-labelled anti-γH2AX antibody, modified with the cell-penetrating peptide, TAT, which includes a nuclear localization sequence.
Methods ^{89}Zr-anti-γH2AX-TAT was synthesized using EDC/NHS chemistry for TAT peptide linkage. Desferrioxamine conjugation allowed labelling with ^{89}Zr. Uptake and retention of ^{89}Zr-anti-γH2AX-TAT was evaluated in the breast adenocarcinoma cell line MDA-MB-468 in vitro or as xenografts in athymic mice. External beam irradiation was used to induce DSBs and expression of γH2AX. Since ^{89}Zr emits ionizing radiation, detailed radiobiological measurements were included to ensure ^{89}Zr-anti-γH2AX-TAT itself does not cause any additional DSBs.
Results Uptake of ^{89}Zr-anti-γH2AX-TAT was similar to previous results using ^{111}In-anti-γH2AX-TAT. Retention of ^{89}Zr-anti-γH2AX-TAT was eightfold higher at 1 h post irradiation, in cells expressing γH2AX, compared to non-irradiated cells or to non-specific IgG control. PET imaging of mice showed higher uptake of ^{89}Zr-anti-γH2AX-TAT in irradiated xenografts, compared to non-irradiated or non-specific controls (12.1±1.6 vs 5.2±1.9 and 5.1±0.8 %ID/g, respectively; $p<0.0001$). The mean absorbed dose to the nucleus of cells taking up ^{89}Zr-anti-γH2AX-TAT was twofold lower compared to ^{111}In-anti-γH2AX-TAT. Additional exposure of neither irradiated nor non-irradiated cells nor tissues to ^{89}Zr-anti-γH2AX-TAT resulted in any significant changes in the number of observable DNA DSBs, γH2AX foci or clonogenic survival.
Conclusion ^{89}Zr-anti-γH2AX-TAT allows PET imaging of DNA DSBs in a tumour xenograft mouse model.

Keywords ^{89}Zr · γH2AX · DNA damage · PET · TAT

James C. Knight and Caitríona Topping contributed equally to this work.

Electronic supplementary material The online version of this article (doi:10.1007/s00259-015-3092-8) contains supplementary material, which is available to authorized users.

✉ Bart Cornelissen
bart.cornelissen@oncology.ox.ac.uk

[1] CRUK/MRC Oxford Institute for Radiation Oncology, Department of Oncology, University of Oxford, Old Road Campus Research Building, Off Roosevelt Drive, Oxford OX3 7LJ, UK

[2] Royal Marsden Hospital, Sutton, Surrey, UK

[3] Facultat de Fisica (ECM and ICC), Universitat de Barcelona, Barcelona, Spain

Introduction

DNA double-strand breaks (DSBs) represent one of the most serious forms of DNA damage. They are the main mechanism through which radiotherapy and some chemotherapeutic agents kill cancer cells [1] and are involved in the genomic instability that lies at the basis of oncogenesis [2]. Despite being a key process of the highest importance to cell homeostasis, methods for the non-invasive in vivo measurement or molecular imaging of the extent of DNA damage or DNA damage repair signalling are not widely available. To date, only two methods exist [3, 4]. Both of these target the phosphorylated DNA damage repair protein, γH2AX [5]. Since

DSBs are not very numerous—20–40 DSBs are induced for every 1 Gy of X-ray absorbed dose [6]—they do not represent a good imaging target. A good alternative, secondary target is one of the earliest and universal events following DSB sensing: the formation of γH2AX (this response is reviewed in detail by Ivashkevich et al. [7]). In human cells, γH2AX is formed when H2AX is phosphorylated on its serine 139 residue by ATM or by other DNA damage response kinases such as ATR or DNA-PKcs [5]. Expressed exclusively in the cell nucleus, γH2AX exists as foci containing up to thousands of copies around the site of DSB damage, making it a more attractive target for non-invasive imaging. After its discovery, the role of H2AX phosphorylation in DNA damage repair and genomic stability was quickly recognized [8, 9] and immunohistochemistry of γH2AX has become a much-used assay in radiobiology [10].

The first reported in vivo imaging method targeting γH2AX involves transfection of cells of interest with recombinant versions of N-terminal and C-terminal halves of luciferase (nLuc and cLuc), fused to H2AX and MDC1, respectively [4]. Upon DSB-induced phosphorylation of H2AX-nLuc, it acts as a binding partner for MDC1-cLuc as part of the MRN complex, which leads to the merger of both halves of luciferase, resulting in a luminescent signal after addition of luciferin. This method is attractive as a high-throughput system for in vitro assays or for imaging DSBs in xenograft animal models. It is however not suited for translation to human subjects.

Previously, we developed the radioimmunoconjugate ^{111}In-anti-γH2AX-TAT and showed that it can be used to quantitatively image DSBs in tumour xenografts in athymic mice [3]. As a single photon emission computed tomography (SPECT) imaging agent, it was demonstrated that the compound was retained in irradiated tumour xenografts, to an extent that was linearly dependent on absorbed radiation dose and the amount of DNA damage, as measured by the number of γH2AX foci. A fluorescently labelled version of anti-γH2AX-TAT co-localized with γH2AX foci in irradiated cancer cells in vitro and in vivo. At higher specific activities (the amount of ^{111}In per gram of compound) the compound can amplify the extent of DSBs and thereby causes inhibition of tumour growth [11]. Furthermore, we applied γH2AX imaging for the very early detection of aplastic lesions in a mouse model of HER2-overexpressing breast cancer [12]. The conjugate used in all of these studies was based on anti-γH2AX antibodies conjugated to the cell-penetrating peptide, TAT (GRKKRRQRRRPPQGYG), which also harbours a nuclear localization sequence [13]. The compound was further modified using a bifunctional metal ion chelator, benzyl-DTPA, to facilitate radiolabelling with ^{111}In, which allows imaging using SPECT.

Given the increasing availability of positron emission tomography (PET) imaging in the clinic and the ability of PET to provide quantitative results, compared to quantitative SPECT imaging where methodology is lagging behind [14], there is a need for a positron-emitting variant of ^{111}In-anti-γH2AX-TAT to aid clinical translation of γH2AX imaging. ^{89}Zr immuno-PET has shown excellent promise in the past few years. Because of its relatively long half-life (78.41 h), ^{89}Zr is an excellent match for the relatively slow pharmacokinetics associated with antibody-based imaging agents.

Here, we report our results on the use of ^{89}Zr-anti-γH2AX-TAT radioimmunoconjugates for the imaging of DNA DSBs in tumour xenograft-bearing mice. In addition, we calculate that, at least on the cellular scale, the radiation dose deposited by ^{89}Zr is smaller compared to ^{111}In. We finally include some in vitro and ex vivo radiobiological observations to establish the superiority of ^{89}Zr-anti-γH2AX-TAT, compared to the ^{111}In-labelled compound.

Materials and methods

Synthesis and radiolabelling

^{89}Zr-labelled anti-γH2AX-TAT was prepared based on previously reported methods [3, 15]. TAT peptide conjugation was achieved using EDC/NHS conjugation chemistry, and desferrioxamine-*p*-SCN was used to allow radiolabelling of the conjugate with ^{89}Zr. Briefly, 100 μg of a rabbit anti-γH2AX antibody (Calbiochem, Nottingham, UK; clone DR1017), which binds both human and mouse γH2AX, was dissolved in 0.1 M 2-(N-morpholino)ethanesulfonic acid (MES) and TAT peptide (GRKKRRQRRRPPQGYG) incorporation was achieved using N-(3-dimethylaminopropyl)-N′-ethylcarbodiimide/N-hydroxysuccinimide (EDC/NHS; Pierce, Rockford, IL, USA) activation. TAT peptide was added in fivefold molar excess for 2 h at room temperature. Unconjugated TAT was removed using Sephadex G-50 gel filtration (SEC) (Bio-Rad, Hemel Hempstead, UK), resulting in a TAT to IgG ratio of 5:1. TAT to IgG-conjugation ratio was determined by radio-iodination of the TAT peptide as previously described [16]. Anti-γH2AX-TAT conjugate, dissolved in sodium bicarbonate buffer (0.1 M, pH 8.5), was incubated with the chelator, desferrioxamine-*p*-SCN (1-(4-isothiocyanatophenyl)-3-[6,17-dihyroxy-7,10,18,21-tetraoxo-27-[N-acetylhydroxylamino)-6,11,17,22-tetraazaheptaeicosane]thiourea; Macrocyclics, Dallas, TX, USA), used at threefold molar excess, for 1 h at room temperature. Excess unreacted desferrioxamine-*p*-SCN was removed by G-50 SEC. $^{89}Zr^{4+}$ (dissolved in 1 M oxalic acid; PerkinElmer, Amsterdam, The Netherlands) was adjusted to neutral pH using 2 M NaOH. Desferrioxamine-conjugated anti-γH2AX-TAT (DFO-anti-γH2AX-TAT) was dissolved in HEPES buffer (0.1 M, pH 7.0) and reacted with appropriate

amounts of ^{89}Zr for 1 h at room temperature, resulting in ^{89}Zr-anti-γH2AX-TAT. Unreacted ^{89}Zr was removed using G-50 SEC, and quality control was performed using instant thin-layer chromatography (ITLC) eluted with sodium citrate buffer (0.1 M, pH 5.0). A similar procedure was followed to produce a control compound based on non-specific IgGs from rabbit serum (rIgG) (Sigma-Aldrich, Dorset, UK), ^{89}Zr-rIgG-TAT.

Optimization of the radiolabelling reaction was performed by evaluating radiolabelling yield using ITLC after reacting varying amounts of DFO-anti-γH2AX-TAT with increasing amounts of ^{89}Zr oxalate. After optimization, radiolabelling yield was routinely >85 %. After purification using G-50 SEC, radiochemical purity was >96 %.

Radioimmunoassays

To confirm the affinity of binding of DFO-anti-γH2AX-TAT to γH2AX, a competition radioimmunoassay (RIA) was performed. MDA-MB-468 cells were irradiated (4 Gy) and incubated for 1 h to allow maximum formation of γH2AX. Biotinylated γH2AX-peptide (Bio-KKATQAS(P)QEY) was used to coat the wells of a streptavidin-coated 96-well plate. ^{111}In-labelled anti-γH2AX (0.2 μg/ml) plus either cold (unlabelled) DFO-anti-γH2AX-TAT or native, unmodified anti-γH2AX in increasing concentrations (range 0–1 μM) were added to the wells. After incubation for 1 h at 37 °C, wells were washed and the radioactivity in each well was determined by quantitative autoradiography. As a control, the same experiments were repeated without the addition of the target peptide, or with addition of a 100-fold excess of γH2AX C-terminal peptide (KKATQAS(P)QEY). To further confirm the affinity of ^{89}Zr-anti-γH2AX-TAT, a saturation binding assay was performed. Increasing concentrations of ^{89}Zr-anti-γH2AX-TAT were added to a 96-well plate with immobilized biotinylated γH2AX-peptide as described above. After a 1-h incubation at 37 °C, the plate was washed and the radioactivity in each well was determined by quantitative autoradiography.

Monte Carlo simulation of dose point kernels

In order to compare the absorbed dose around ^{89}Zr with that of ^{111}In, the respective dose point kernels of isotropic point sources placed in an infinite liquid water medium were simulated using the general-purpose Monte Carlo code PENELOPE [17]. The electron energy spectra of these radionuclides were obtained from Eckerman and Endo [18]. Detailed (event-by-event) simulation of electrons was performed with electron cut-off energies set to 50 eV. The absorbed dose was scored in 1-nm-thick spherical shells around the decay site of ^{89}Zr and ^{111}In. A total of 2×10^9 primary particles were simulated in each run with a statistical uncertainty (2 SD) less than 0.1 %.

In vitro evaluation

MDA-MB-468 human breast adenocarcinoma cells were obtained from ATCC. Cells were tested and authenticated by the provider, and were used no longer than 6 months after retrieval from liquid nitrogen storage. Cells were cultured in 5 % CO_2 in DMEM cell culture medium (Sigma-Aldrich, Dorset, UK), supplemented with 10 % fetal calf serum (Invitrogen, Paisley, UK), and penicillin/streptomycin, 100 units/ml (Invitrogen, Paisley, UK).

Cell uptake and in vitro radiobiology assays

To determine the effect of radiation damage to internalization of ^{89}Zr-IgG-TAT conjugates, aliquots of 2×10^5 MDA-MB-468 cells were seeded in 24-well plates in 500 μl of cell growth medium and allowed to adhere overnight. Cells were exposed to ^{89}Zr-anti-γH2AX-TAT or ^{89}Zr-rIgG-TAT (0.25 μg/ml, 0.5 MBq/μg) for 1 h at 37 °C, irradiated using a ^{137}Cs source (4 Gy, 1 Gy/min) or mock-irradiated (0 Gy) and incubated for a further hour. Cells were washed with 0.25 M glycine-HCl in order to remove membrane-bound compound, washed and lysed using 0.1 M NaOH and the amount of cell-associated ^{89}Zr was determined by automated gamma counting [16].

The influence of DNA damage on the retention of ^{89}Zr-anti-γH2AX-TAT in cells was determined by a load-and-chase experiment, in a similar fashion as previously reported [3]. MDA-MB-468 cells were exposed to ^{89}Zr-anti-γH2AX-TAT or ^{89}Zr-rIgG-TAT (0.25 μg/ml, 0.5 MBq/μg) for 1 h at 37 °C. Cells were then irradiated using a ^{137}Cs source (4 Gy, 1 Gy/min) or mock-irradiated (0 Gy) and incubated for a further hour. Growth medium was then removed, cells were washed and supplied with fresh growth medium. After incubation at 37 °C for another hour, the amount of cell-associated ^{89}Zr was determined by lysis of the cells with 0.1 N NaOH as described above. The amount of ^{89}Zr associated with the cell membrane, cytoplasm or nucleus of cells was determined by cell fractionation as previously described [16]. Detailed methodology is laid out in the supplementary information.

Since the use of radionuclides can in itself lead to the formation of DNA damage, the extent of DSBs after exposure to ^{89}Zr-anti-γH2AX-TAT was measured by counting γH2AX foci. MDA-MB-468 cells were exposed to ^{89}Zr-anti-γH2AX-TAT or ^{89}Zr-rIgG-TAT (0.25 μg/ml, 0.5 MBq/μg) for 1 h at 37 °C. Then, cells were irradiated using a ^{137}Cs source (4 Gy, 1 Gy/min) or mock-irradiated (0 Gy), incubated for 1 further hour and stained for γH2AX as previously described, using monoclonal mouse anti-γH2AX antibodies and fluorescently labelled goat anti-mouse IgGs [3]. Microscopy was performed using a Zeiss 750 confocal microscope, and the number of γH2AX foci per cells was determined in at least 100 cells.

Since γH2AX foci are a secondary marker of DNA damage, the extent of DSB damage was also measured by neutral comet assay. Cells were treated as above, and comet assays were performed as previously described [11]. Additionally, the effect of ^{89}Zr-anti-γH2AX-TAT or ^{89}Zr-rIgG-TAT on clonogenic survival was studied. Cells were treated as above, seeded in 6-well plates and supplied with DMEM with 20 % fetal bovine serum (FBS). After 14 days, cells were washed, stained with methylene blue (1 % in a methanol:water 1:1 mixture), and the number of colonies was counted.

Microdosimetry

To compare the absorbed dose in the nucleus of cancer cells treated with ^{89}Zr-anti-γH2AX-TAT or ^{111}In-anti-γH2AX-TAT, the MIRD formalism for cellular dosimetry was adopted [19]. Detailed methodology is laid out in the supplementary information. To determine the amount of activity in each cell compartment, fractionation of MDA-MB-468 cells, 1 h after exposure to 0.25 μg/ml ^{89}Zr-anti-γH2AX-TAT (0.5 MBq/μg, 0.25 μg/ml) or ^{111}In-anti-γH2AX-TAT (0.5 MBq/μg, 0.25 μg/ml), was performed as previously described [20].

In vivo studies

All animal procedures were carried out in accordance with the UK Animals (Scientific Procedures) Act 1986 and with local Ethics Committee approval. MDA-MB-468 xenografts were established in the right flank of female athymic BALB/c *nu/nu* mice (Harlan, UK). After 3 weeks, tumours developed an average size of 800 μl and were used for PET/CT imaging. ^{89}Zr-anti-γH2AX-TAT or ^{89}Zr-rIgG-TAT (5 μg, 0.5 MBq) were administered intravenously. γH2AX was induced by irradiation of the tumour (10 Gy), 1 h after injection of the imaging probe. Radiation was delivered using a Gulmay 320 kV X-irradiator, 2.0 Gy/min. As a control, some mice were mock-treated (0 Gy). For PET/CT imaging, mice were anaesthetized using 2–4 % isoflurane in air at 24 h after injection of the radiopharmaceutical. PET/CT imaging was performed using the Inveon PET/CT scanner (Siemens). Volume of interest (VOI) analysis was performed using the Inveon Research Workplace software package (Siemens). VOIs were drawn around the major organs and the tumour. A VOI drawn around the heart served as a measure for radioactivity in the blood. After PET imaging, mice were euthanized and blood, tumour and selected organs were removed, weighed and counted for radioactivity. In order to evaluate the influence of the use of radioactive ^{89}Zr on the number of DNA repair foci, 10-μm-thick sections of tumour tissue were prepared, which were stained for γH2AX foci as previously described [3]. Three to six animals were evaluated per group.

Statistical analyses

All statistical analyses and non-linear regression were performed using GraphPad Prism (GraphPad Software Inc). One- or two-way analysis of variance (ANOVA) was used for multiple comparisons, with Tukey post hoc tests to calculate significance of differences between groups.

Results

Synthesis

Optimization of the radiolabelling reaction was performed by evaluating radiolabelling yield using ITLC after reacting varying amounts of DFO-anti-γH2AX-TAT with increasing amounts of ^{89}Zr oxalate. Results of these optimization efforts are summarized in Supplementary Figure S1A-C. After optimization, radiolabelling yield was routinely >85 %. After purification using G-50 SEC, radiochemical purity was >96 %, as determined using ITLC and G-50 SEC (Supplementary Figure S1D).

To confirm the affinity of binding of DFO-anti-γH2AX-TAT to native, unmodified anti-γH2AX, a competition radioimmunoassay was performed (Fig. 1a). The results showed that the ability of DFO-conjugated anti-γH2AX-TAT to compete with ^{111}In-labelled anti-γH2AX antibody was only slightly lower compared to native, unmodified anti-γH2AX (IC_{50} (95 % confidence interval)=0.044 (0.042–0.049) vs 0.027 (0.025–0.029) nM, respectively; p=0.0001). This ratio was not significantly different to that previously obtained using DTPA-conjugated anti-γH2AX-TAT (p>0.05) [3]. Binding of radiolabelled anti-γH2AX to immobilized γH2AX peptide was blocked using a competing amount of soluble γH2AX-mimicking peptide (p<0.0001; Fig. 1b). Prevention of specific binding by omitting the target peptide significantly reduced the binding of radiolabelled anti-γH2AX (p <0.0001; Fig. 1c). Saturation binding assay showed a K_d of 5.14±0.31 nM (Fig. 1d).

Cell uptake studies

Internalization of radiolabelled compound into MDA-MB-468 cells was evaluated by removal of all non-cell-associated radioactivity by washing the cells and removal of any membrane-associated compound by acid wash. Internalization of ^{89}Zr-IgG-TAT into MDA-MB-468 cells was similar to that observed for ^{111}In-mouse IgG-TAT [16] (Fig. 2a). Some degree of saturation was observed at later time points. Similar to ^{111}In-anti-γH2AX-TAT, no significant differences were observed between the internalization of ^{89}Zr-anti-γH2AX-TAT in irradiated or unirradiated cells, or compared to ^{89}Zr-rIgG-TAT (p=0.5881) (Fig. 2b).

Retention of radiolabelled compound in MDA-MB-468 cells was evaluated using a load-and-chase experiment. The

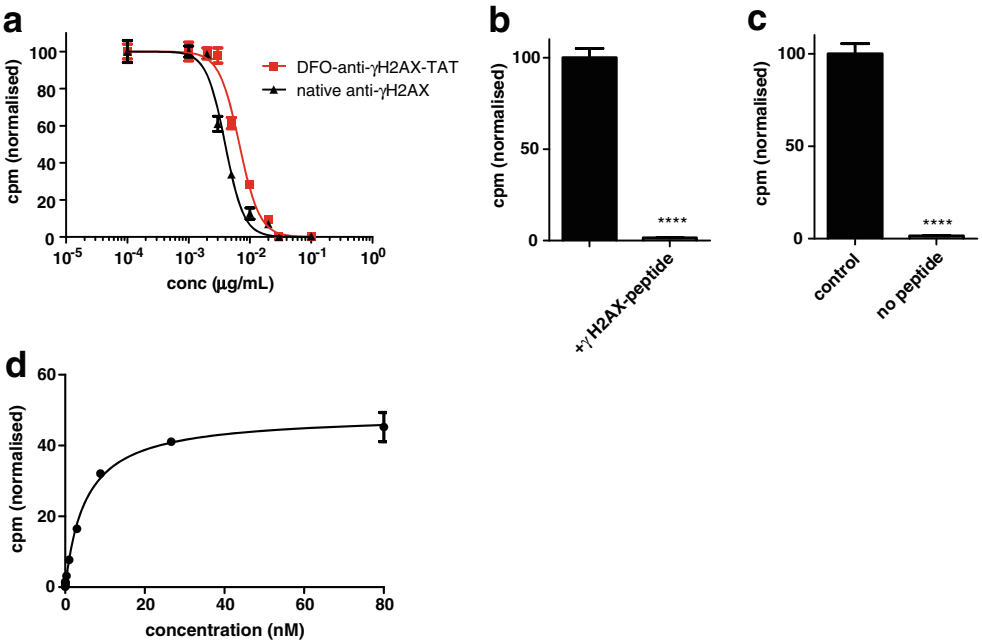

Fig. 1 **a** Radioimmunoassays showed that the ability of DFO-conjugated anti-γH2AX-TAT to compete with ^{111}In-labelled anti-γH2AX for binding to an immobilized γH2AX-mimicking peptide was not significantly different from native, unmodified anti-γH2AX. **b** Addition of soluble γH2AX-mimicking peptide abolished binding of the radiolabelled anti-γH2AX. **c** Omission of immobilized γH2AX-mimicking target peptide significantly reduced the binding of radiolabelled anti-γH2AX. **d** Saturation binding of ^{89}Zr-anti-γH2AX-TAT on immobilized γH2AX-mimicking target peptide

retention of ^{89}Zr-anti-γH2AX-TAT, measured as the relative amount of cell-associated ^{89}Zr remaining after a 1-h chase, was significantly higher in irradiated cells compared to ^{89}Zr-rIgG-TAT in irradiated MDA-MB-468 cells (14.79±1.75 % vs 1.88±0.25 %; $p<0.001$) (Fig. 2c). In non-irradiated cells, 3.76±0.40 % of ^{89}Zr-anti-γH2AX-TAT was retained, significantly less compared to irradiated cells ($p<0.001$).

Taken together, the internalization and retention results suggest that signal to background contrast can be generated through prolonged retention of ^{89}Zr-anti-γH2AX-TAT in the cells which express the target, γH2AX, a result comparable to that obtained using ^{111}In-anti-γH2AX-TAT [3].

In vivo imaging and biodistribution

To test the ability of ^{89}Zr-anti-γH2AX-TAT RIC to visualize DNA damage in vivo, MDA-MB-468 xenograft-bearing mice were imaged using a small animal dedicated PET camera, 24 h

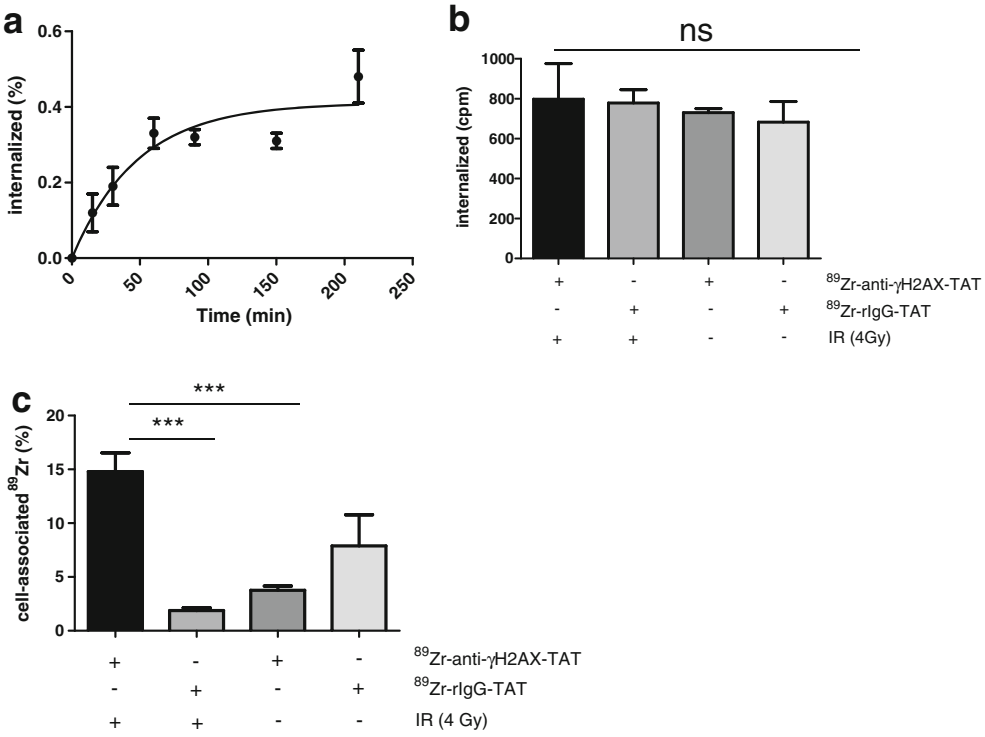

Fig. 2 **a** Internalization of ^{89}Zr-anti-γH2AX-TAT into MDA-MB-468 cells. **b** Internalization of ^{89}Zr-anti-γH2AX-TAT or ^{89}Zr-rIgG-TAT into irradiated or non-irradiated MDA-MB-468 cells. No significant changes were observed. **c** The cell-associated amount of ^{89}Zr remaining after a 1-h interval (expressed as a percentage of the cell-associated amount of ^{89}Zr after a 1-h incubation) is significantly higher for ^{89}Zr-anti-γH2AX-TAT in irradiated MDA-MB-468 cells, compared to non-specific ^{89}Zr-rIgG-TAT control compound and compared to non-irradiated cells

following administration of ^{89}Zr-anti-γH2AX-TAT or ^{89}Zr-rIgG-TAT. Transverse images through tumours are shown in Fig. 3a, and coronal sections are shown in Supplementary Figure S5. VOI analyses of tumours were performed (Fig. 3b), showing significantly higher tumour uptake of ^{89}Zr-anti-γH2AX-TAT in irradiated xenograft tumours compared to non-irradiated tumours or control compound ^{89}Zr-rIgG-TAT (uptake was 12.1±1.6 %ID/g vs 5.3±1.9 %ID/g and 5.1±0.8 %ID/g, respectively; p=0.0057). Tumour to heart and tumour to muscle ratios were calculated and were significantly higher for ^{89}Zr-anti-γH2AX-TAT in irradiated tumours compared to control (Fig. 3c). Bone uptake was also observed (Supplementary Figure S5), amounting to 11 %ID/g (Fig. 3b) which is ascribed to the presence of a small amount of free ^{89}Zr in the preparation of ^{89}Zr-anti-γH2AX-TAT used for imaging.

Following acquisition of images mice were euthanized and selected organs removed and counted for radioactivity. These necropsy data confirmed significant retention of ^{89}Zr-anti-γH2AX-TAT, but not ^{89}Zr-rIgG-TAT in irradiated tumours (Fig. 4). Uptake of ^{89}Zr in irradiated tumours at 24 h after administration of ^{89}Zr-anti-γH2AX-TAT was 6.07±1.16 %ID/g, significantly higher compared to non-irradiated tumours or ^{89}Zr-rIgG-TAT (4.21±0.33 or 2.36±0.88 %ID/g, respectively; p<0.0021). One noteworthy observation is the significantly lower amount of ^{89}Zr-anti-γH2AX-TAT in the blood of radiation-treated animals, resulting in a tumour to blood ratio of 11.1±6.8. This was significantly higher than in unirradiated controls or animals that were administered the control compound ^{89}Zr-rIgG-TAT (0.59±0.23 and 1.05±1.03, respectively; p=0.02). Uptake in other tissues, or in the whole body, was not significantly different, except for well-perfused organs such as liver and lung, which may be ascribed to the differences in the blood.

Radiobiological studies and microdosimetry

The deposited dose around a decaying ^{89}Zr or ^{111}In nuclide was calculated using Monte Carlo simulation (Supplementary Figure S2). Taking into account all potential emissions, including Auger and Coster-Kronig electrons, internal conversion electrons and beta particles, the calculated mean absorbed dose to the nucleus caused by emissions from the nucleus, cytoplasm and cell surface per decay (i.e. the S-value) was substantially less for ^{89}Zr (p=0.0713). The gamma emissions for both isotopes were omitted as they contributed less than 2 % to the calculated S-values.

Fractionation of MDA-MB-468 cells exposed to ^{89}Zr-anti-γH2AX-TAT for 1 h revealed similar results compared to those using ^{111}In-anti-γH2AX-TAT (p<0.05) (Table 1). S-values for ^{89}Zr and ^{111}In were calculated (Table 1). Dosimetry using a like-for-like comparison (similar starting activities and concentrations) showed that ^{89}Zr-anti-γH2AX-TAT exposure gives rise to an absorbed dose of 85 mGy, compared to 166 mGy for the ^{111}In-labelled compound, an approximately twofold difference.

Counting the number of γH2AX foci in cells exposed to ^{89}Zr-anti-γH2AX-TAT revealed no significant increase when compared to untreated cells. The number of foci was increased by gamma irradiation as expected (up to 12-fold after a

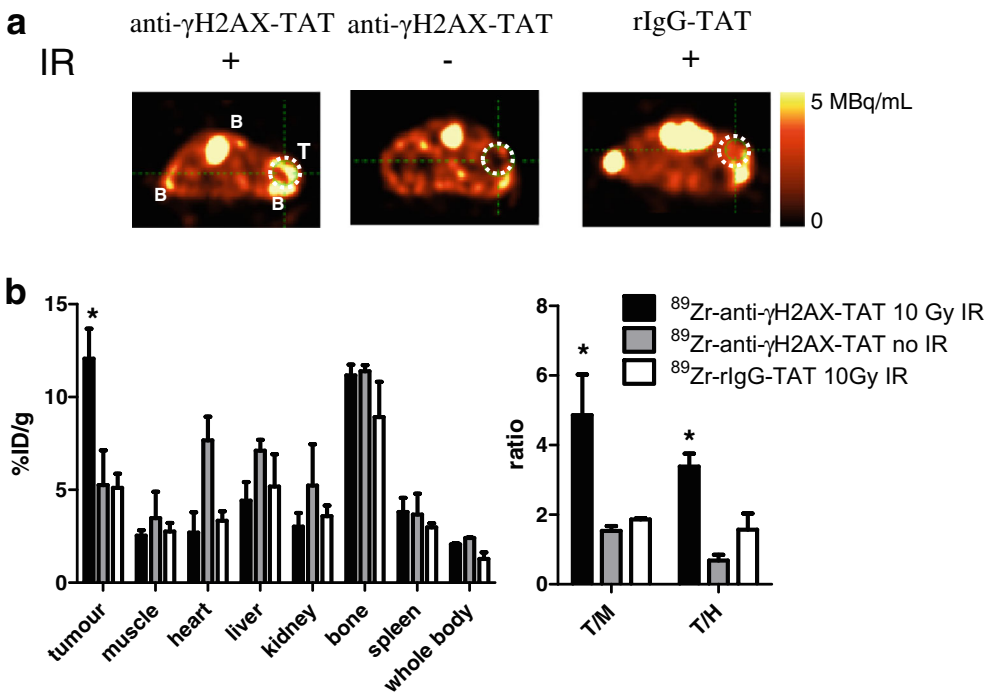

Fig. 3 **a** Representative PET images of mice, 24 h after intravenous administration of ^{89}Zr-anti-γH2AX-TAT or ^{89}Zr-rIgG-TAT in xenograft-bearing mice, with irradiated or non-irradiated xenografts. Transverse sections through the tumour (*white circles*) are shown. *T* tumour, *B* bone. **b** VOI analysis of selected tissues of PET images. The VOI drawn around the heart represents the activity in the heart muscle and the blood. Tumour to heart (*T/H*) and tumour to muscle (*T/M*) ratios were calculated (n=3 per group)

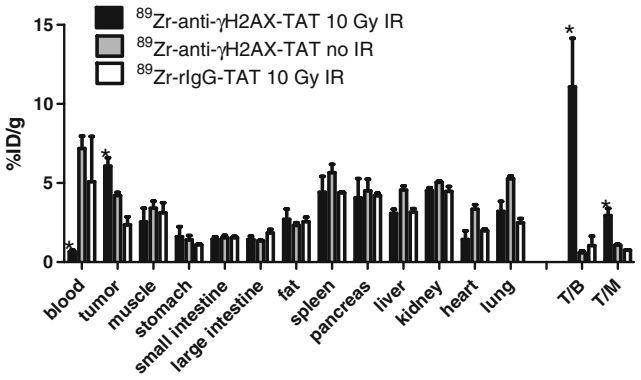

Fig. 4 Biodistribution of ^{89}Zr, 24 h post injection of ^{89}Zr-anti-γH2AX-TAT or ^{89}Zr-rIgG-TAT in xenograft-bearing mice, with irradiated or non-irradiated xenografts. Blood and major tissues are shown, including tumour to blood (*T/B*) and tumour to muscle (*T/M*) ratios (n=3–6 per group)

radiation dose of 6 Gy; $p<0.0001$) (Fig. 5a), but additional exposure to ^{89}Zr-anti-γH2AX-TAT, ^{89}Zr-rIgG-TAT or non-radiolabelled controls did not significantly increase the number of foci per cell ($p>0.05$).

Clonogenic survival of MDA-MB-468 cells was significantly decreased by gamma irradiation (4 Gy). The number of colonies decreased by 60 % after irradiation ($p<0.0001$) (Fig. 5b). However, additional exposure of cells to rIgG-TAT, anti-γH2AX-TAT, ^{89}Zr-anti-γH2AX-TAT or ^{89}Zr-rIgG-TAT did not lead to an additional decrease in clonogenic survival in either irradiated or non-irradiated cells ($p>0.05$).

Neutral comet assays were used to study the effects of ^{89}Zr-anti-γH2AX-TAT on DSBs directly. Even though the number of γH2AX foci was not significantly affected, DNA repair foci are a secondary measure for the extent of DSB damage. Comet assays showed a significant increase in the level of DSB damage by gamma irradiation (3 or 6 Gy, compared to unirradiated cells; $p<0.0001$), but no statistically significant changes in the number of DSBs after exposure to either ^{89}Zr-anti-γH2AX-TAT or ^{89}Zr-rIgG-TAT in either irradiated or non-irradiated cells ($p>0.05$) (Fig. 5c).

Irradiation (10 Gy) of tumour tissue caused a significant increase in the number of γH2AX foci per cell (from 12.9±1.8 to 71.5±4.5 foci/cell; $p<0.001$); however, no additional γH2AX foci were observed in tumour sections from mice exposed to ^{89}Zr-anti-γH2AX-TAT compared to control compounds, neither in irradiated tumour tissue nor in unirradiated tissue ($p>0.05$) (Supplementary Figure S3).

Discussion

True personalized medicine in oncology can only be possible with the development of new imaging agents that will enable molecular staging of tumours, to predict, guide and monitor treatment. PET, CT and MRI, alone or in combination, could represent a step toward non-invasive imaging for patient stratification and individualized chemotherapy [21]. PET imaging has already delivered on its great potential for imaging in oncology, as agents have been developed against most of the hallmarks of cancer, even though many methods have yet to make the translation from basic research to clinical practice [22]. Radiopharmaceuticals have been developed to target angiogenesis, cell death, increased metabolism and energetics, increased proliferation/immortality, proliferative signalling, metastasis and invasion, and tumour-promoting inflammation [23], but only one agent existed to date to target DNA damage [3].

Here, we describe the use of ^{89}Zr-anti-γH2AX-TAT, a positron-emitter-labelled variant of the previously described ^{111}In-labelled agent used for SPECT imaging [12, 3]. The need for an alternative for PET imaging is motivated by the increased use of PET versus SPECT in oncology research and the acceptance of PET/CT as the standard of care [24]. Moreover, clinical PET is quantifiable. Even though implementation of accurate attenuation correction had been anticipated a decade ago, clinical SPECT systems generally remain unable to provide quantitative information [25]. Our efforts to develop a positron-emitting version of the anti-γH2AX-TAT antibody construct based on our previously reported ^{111}In-labelled version resulted in notable differences in the chemical and radioactive properties. The most obvious of these is the conjugation of two distinct radiometal complexes, ^{111}In-

Table 1 Cellular S-values (mGy/Bq s) for MDA-MB-468 cells, as calculated using the MIRD formalism (using R_C=9.5 μm and R_N=6.7)

	S-values (Gy/Bq s)			Activity (kBq)[a]			Nuclear dose (mGy)
Radionuclide	S(N←N)	S(N←Cy)	S(N←CS)	Nucleus	Cytoplasm	Surface	
^{89}Zr	5.09 10^{-04}	5.45 10^{-05}	1.40 10^{-05}	22.06±0.09	8.82±0.03	6.62±0.04	85.0±0.11
^{111}In	7.07 10^{-04}	8.12 10^{-05}	4.25 10^{-05}	22.8±0.3	8.08±0.02	6.63±0.01	165.7±0.30

Activities of ^{89} Zr and ^{111} In measured on the cell surface, in the cytoplasm and in the nucleus of MDA-MB-468 cells and mean absorbed radiation dose to the nucleus (nuclear dose), calculated based on S-values and activities

N nucleus, *Cy* cytoplasm, *CS* cell surface

[a] Accumulated activity was determined as the product of activity (in 500,000 cells) and incubation time (1 h)

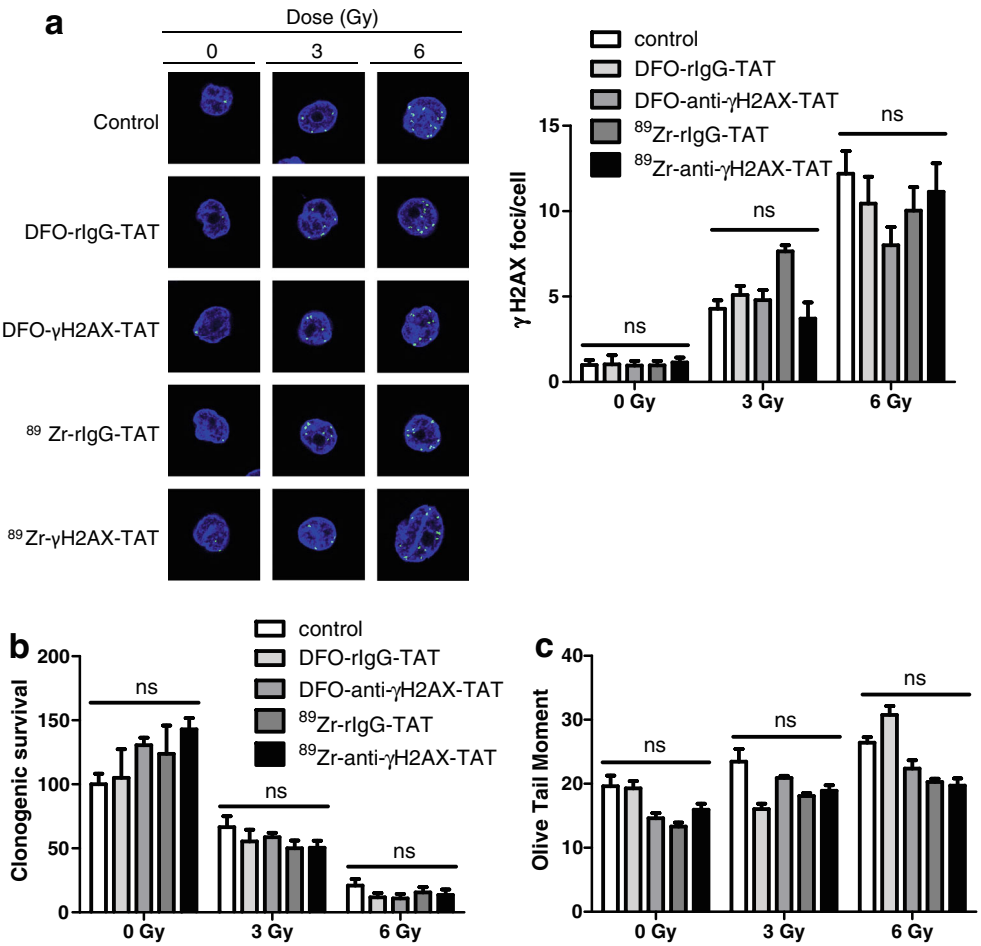

Fig. 5 **a** The number of γH2AX foci was determined using immunohistochemistry in MDA-MB-468 cells after exposure to irradiation (0 or 4 Gy) combined with phosphate-buffered saline (PBS) or ^{89}Zr-labelled or unlabelled anti-γH2AX-TAT, or rIgG-TAT. **b** Clonogenic survival of MDA-MB-468 cells after exposure to irradiation (0 or 4 Gy) combined with PBS or ^{89}Zr-labelled or unlabelled anti-γH2AX-TAT, or rIgG-TAT. **c** Olive tail moment was determined after a neutral comet assay on MDA-MB-468 cells after exposure to irradiation (0 or 4 Gy) combined with PBS or ^{89}Zr-labelled or unlabelled anti-γH2AX-TAT, or rIgG-TAT

DTPA and ^{89}Zr-DFO, which provide differences in, for example, charge, molecular weight, lipophilicity etc. It is likely, however, that these variations are rendered negligible when considering the large disparity in size between the radiometal complex and the antibody to which it is bound, the latter of which most likely dominates the overall chemical properties of the whole construct. Another notable difference is that for in vivo imaging experiments, ^{89}Zr-anti-γH2AX-TAT was labelled at a lower specific activity compared to the ^{111}In-anti-γH2AX-TAT imaging agent (0.1 MBq/μg and 0.5 MBq/μg, respectively). This is made possible by the increased sensitivity of PET versus SPECT, which enables images of comparable quality to be acquired despite using lower quantities of the radioactive probe. We predict that this will provide advantages in terms of reducing radiation burden to patients, their families and carers, and medical staff, although we did not perform these calculations in the present study.

Promisingly, despite these differences, the ^{89}Zr-labelled anti-γH2AX-TAT antibody construct revealed highly comparable radiobiological behaviour compared with the analogous ^{111}In-labelled version. Firstly, in a similar manner to the ^{111}In-labelled construct, ^{89}Zr-anti-γH2AX-TAT also exhibits more prolonged retention inside MDA-MB-468 breast cancer cells in vitro following gamma irradiation compared with control experiments. It is this prolonged retention inside cells with damaged DNA which is the critical factor in determining the performance of ^{89}Zr-anti-γH2AX-TAT as an in vivo imaging agent as it results in higher concentrations of radioactivity in tumours compared to surrounding tissues. BALB/c *nu*/*nu* mice, which are not radiosensitive, were used for this series of experiments [26–28]. Since DNA damage repair is relatively fast in normal tissues, little γH2AX remains several hours after irradiation, leaving little target for the radiolabelled anti-γH2AX-TAT compound to engage, resulting in little uptake of ^{89}Zr-anti-γH2AX-TAT in normal irradiated tissues. The single tissue to receive a significant amount of radiation dose is the hind leg at the side of tumour implantation, but no significantly increased uptake of either ^{111}In- or ^{89}Zr-anti-γH2AX-TAT has been observed using SPECT or PET imaging, respectively [3].

Furthermore, cell fractionation studies also indicate that the distribution of the two imaging agents inside irradiated cells was almost identical after 1 h incubation (Table 1) which confirms that the modification of the antibody with ^{89}Zr-DFO radiometal complex did not impede its ability to localize in the cell nucleus compared with the ^{111}In-labelled variant.

Surprisingly, we observed a significant decrease in the amount of ^{89}Zr measured in the blood of mice with irradiated tumours and injected with ^{89}Zr-anti-γH2AX-TAT resulting in higher tumour to blood values compared to ^{111}In-anti-γH2AX-TAT. Although this phenomenon is yet to be fully elucidated, we hypothesize that this decrease may be the result of a combination of sequestration of radiolabelled compound from the blood to tumour tissue and ^{89}Zr biodistribution (Supplementary Figure S4). No other significant differences were observed between the different animal groups, such as in the bone, suggesting that the lowered blood radioactivity in irradiated mice was not due to additional sequestration of ^{89}Zr to the bone ($p>0.05$), nor was it the result of increased excretion (whole body measurements, $p>0.05$). The drop in %ID in the blood [a difference (Δ) of 6.52 %ID in irradiated versus non-irradiated animals injected with ^{89}Zr-anti-γH2AX-TAT] can mainly be explained by a shift to tumour (Δ=−2.36 %ID), the kidneys and bladder (Δ=−2.97 %ID), with the remainder of the dose moved to various other organs. However, the mechanism of this shift is not clear, especially since no difference was observed in terms of excretion from the whole body. Future investigations will be the subject of further reports on this intriguing matter.

Targeting of γH2AX by agents such as ^{89}Zr-anti-γH2AX-TAT may provide a solution for visualizing the changes during early tumourigenesis, the inherent genomic instability, the intrinsic lack of DNA damage repair in existing tumours and reaction of tissue to anti-tumour therapy. Applications of DNA damage imaging are nearly as manifold as the use of H2AX phosphorylation as a histology biomarker [7]. Imaging has the added advantage of being a non-invasive, repeatable technique able to visualize DNA damage throughout the whole body, whether it be in mice for the purpose of translational research or in cancer patients for clinical benefit. Firstly, applications of DNA damage imaging could be envisioned in early detection of tumours, which had been anticipated nearly a decade ago [8]. We have used the DNA damage repair response to oncogenic stress in a mmtv-driven neuT-overexpressing mouse model of breast cancer [12]. Furthermore, DNA damage imaging could aid tumour diagnosis. In some cases, overexpression of γH2AX is even a better histological marker than the gold standard method, as is the case for metastatic renal cell carcinoma, where markers such as RCC marker, have been employed with varying success [29]. Also, γH2AX imaging may be used as an aid for staging or use as a prognostic biomarker, by determining genetic instability of diagnosed tumours [8, 9, 30] or hypersensitivity of normal tissues [31, 27]. Finally, imaging DSBs using PET has applications in therapy evaluation of chemo- and radiotherapy, where short-term individualized window studies could shed light on the usefulness of treatments or treatment combinations [7, 32, 33].

A potential limitation of PET imaging of DSBs is that the ionizing radiation emitted from the decaying radionuclide could itself be causing additional DNA damage, which would hamper the use of ^{89}Zr-anti-γH2AX-TAT as a radiotracer. This effect has been apparent in previous studies involving ^{111}In-anti-γH2AX-TAT when radiolabelled at specific activities greater than 3 MBq/μg, and therefore it was necessary in this study to explore this possibility [11, 34, 35]. Furthermore, unlabelled anti-γH2AX-TAT binds to the same phosphorylated serine residue on the H2AX protein needed as a docking site for activation of other DNA damage repair proteins. Therefore, occupation of this site by an excess of imaging agent may lead to DNA damage repair abrogation, and further genomic instability or cell death [36, 37]. Given these conceivable side effects, it was necessary to investigate the effects of unlabelled and ^{111}In- and ^{89}Zr-labelled anti-γH2AX-TAT in silico and in vitro, in MDA-MB-468 cells. High concentrations of unlabelled anti-γH2AX-TAT slow down γH2AX foci formation, but have no effect on the resolution of DSBs, as shown by the neutral comet assay (data not shown). We previously showed that ^{111}In-anti-γH2AX-TAT, labelled with low amounts of ^{111}In necessary for imaging (<1 MBq/μg), similar to ^{89}Zr-anti-γH2AX-TAT, also does not affect DSB repair in vitro [11] or cause tumour growth delay in vivo [12]. In this manuscript, we show that this is also the case for the ^{89}Zr-labelled version, even though the spectrum of emitted particles includes more energetic gamma rays and a beta particle as well as low-energy electrons. We conclude from these calculations that even if ^{89}Zr-anti-γH2AX-TAT was radiolabelled at the same specific activity as the ^{111}In-labelled variant, it is less likely to cause the same degree of DNA damage. This potential side effect was further examined experimentally where a lack of difference in γH2AX foci formation was observed in cells which were either incubated with ^{89}Zr-anti-γH2AX-TAT (0.5 MBq/μg) or left untreated. These results are in keeping with similar experiments involving the ^{111}In-labelled variant when labelled at the same specific activity. Neutral comet assays, clonogenic assays in vitro and measurements of the number of γH2AX foci in vivo all corroborated these findings. Although these results are promising on the single-cell level, additional calculations and measurements are necessary to study dosimetry on the whole body scale. These will be the subject of further reports.

Conclusion

Taken together, ^{89}Zr-anti-γH2AX-TAT allows in vivo PET imaging of DNA DSB damage in a mouse model of cancer. In silico modelling showed that the mean absorbed dose to the nucleus of cells taking up ^{89}Zr-anti-γH2AX-TAT was twofold lower compared to ^{111}In anti-γH2AX-TAT. In vitro and ex vivo analysis showed that exposure of naïve or irradiated cells or xenograft tumour tissue to ^{89}Zr-anti-γH2AX-TAT did

not significantly change the number of DNA DSBs, the number of γH2AX foci or clonogenic survival.

Acknowledgments The authors sincerely thank Prof. Nicola R. Sibson, Prof. Katherine A. Vallis, and Dr. Sean Smart for their support. We further thank Cancer Research UK, MRC, the Oxford Cancer Research Centre and the CRUK&EPRSC Cancer Imaging Centre in Oxford for financial support.

Ethical approval All applicable international, national and/or institutional guidelines for the care and use of animals were followed.

Conflicts of interest None.

References

1. Helleday T, Petermann E, Lundin C, Hodgson B, Sharma RA. DNA repair pathways as targets for cancer therapy. Nat Rev Cancer 2008;8(3):193–204. doi:10.1038/nrc2342.
2. Bartek J, Bartkova J, Lukas J. DNA damage signalling guards against activated oncogenes and tumour progression. Oncogene 2007;26(56):7773–9. doi:10.1038/sj.onc.1210881.
3. Cornelissen B, Kersemans V, Darbar S, Thompson J, Shah K, Sleeth K, et al. Imaging DNA damage in vivo using gammaH2AX-targeted immunoconjugates. Cancer Res 2011;71(13):4539–49. doi:10.1158/0008-5472.CAN-10-4587.
4. Li W, Li F, Huang Q, Shen J, Wolf F, He Y, et al. Quantitative, noninvasive imaging of radiation-induced DNA double-strand breaks in vivo. Cancer Res 2011;71(12):4130–7. doi:10.1158/0008-5472.CAN-10-2540.
5. Rogakou EP, Pilch DR, Orr AH, Ivanova VS, Bonner WM. DNA double-stranded breaks induce histone H2AX phosphorylation on serine 139. J Biol Chem 1998;273(10):5858–68.
6. Rothkamm K, Löbrich M. Evidence for a lack of DNA double-strand break repair in human cells exposed to very low x-ray doses. Proc Natl Acad Sci U S A 2003;100(9):5057–62. doi:10.1073/pnas.0830918100.
7. Ivashkevich A, Redon CE, Nakamura AJ, Martin RF, Martin OA. Use of the gamma-H2AX assay to monitor DNA damage and repair in translational cancer research. Cancer Lett 2012;327:123–33. 10.1016/j.canlet.2011.12.025. doi:10.1016/j.canlet.2011.12.025.
8. Bartkova J, Horejsí Z, Koed K, Krämer A, Tort F, Zieger K, et al. DNA damage response as a candidate anti-cancer barrier in early human tumorigenesis. Nature 2005;434(7035):864–70. doi:10.1038/nature03482.
9. Celeste A, Petersen S, Romanienko PJ, Fernandez-Capetillo O, Chen HT, Sedelnikova OA, et al. Genomic instability in mice lacking histone H2AX. Science 2002;296(5569):922–7. doi:10.1126/science.1069398.
10. Shah K, Cornelissen B, Kiltie AE, Vallis KA. Can γH2AX be used to personalise cancer treatment? Curr Mol Med 2013;13(10):1591–602.
11. Cornelissen B, Darbar S, Kersemans V, Allen PD, Falzone N, Barbeau J, et al. Amplification of DNA damage by a γH2AX-targeted radiopharmaceutical. Nucl Med Biol 2012;39(8):1142–51. doi:10.1016/j.nucmedbio.2012.06.001.
12. Cornelissen B, Able S, Kartsonaki C, Kersemans V, Allen D, Cavallo F, et al. Imaging DNA damage allows detection of preneoplasia in the BALB-neuT model of breast cancer. J Nucl Med 2014;55(12):2026–31. doi:10.2967/jnumed.114.142083.
13. Kersemans V, Kersemans K, Cornelissen B. Cell penetrating peptides for in vivo molecular imaging applications. Curr Pharm Des 2008;14(24):2415–47.
14. Bailey DL, Willowson KP. An evidence-based review of quantitative SPECT imaging and potential clinical applications. J Nucl Med 2013;54(1):83–9. doi:10.2967/jnumed.112.111476.
15. Vosjan MJ, Perk LR, Visser GW, Budde M, Jurek P, Kiefer GE, et al. Conjugation and radiolabeling of monoclonal antibodies with zirconium-89 for PET imaging using the bifunctional chelate p-isothiocyanatobenzyl-desferrioxamine. Nat Protoc 2010;5(4):739–43. doi:10.1038/nprot.2010.13.
16. Cornelissen B, Hu M, McLarty K, Costantini D, Reilly RM. Cellular penetration and nuclear importation properties of 111In-labeled and 123I-labeled HIV-1 tat peptide immunoconjugates in BT-474 human breast cancer cells. Nucl Med Biol 2007;34(1):37–46. doi:10.1016/j.nucmedbio.2006.10.008.
17. Salvat F, Fernández-Varea JM, Sempau J, editors. PENELOPE: a code system for Monte Carlo simulation of electron and photon transport. OECD Nuclear Energy Agency; 2011; Issy-les-Moulineaux.
18. Eckerman KF, Endo A. MIRD: radionuclide data and decay schemes. Reston: Society of Nuclear Medicine; 2008.
19. Goddu SM, Howell RW, Rao DV. Cellular dosimetry: absorbed fractions for monoenergetic electron and alpha particle sources and S-values for radionuclides uniformly distributed in different cell compartments. J Nucl Med 1994;35(2):303–16.
20. Cornelissen B, McLarty K, Kersemans V, Scollard DA, Reilly RM. Properties of [(111)In]-labeled HIV-1 tat peptide radioimmunoconjugates in tumor-bearing mice following intravenous or intratumoral injection. Nucl Med Biol 2008;35(1):101–10. doi:10.1016/j.nucmedbio.2007.09.007.
21. Laing RE, Walter MA, Campbell DO, Herschman HR, Satyamurthy N, Phelps ME, et al. Noninvasive prediction of tumor responses to gemcitabine using positron emission tomography. Proc Natl Acad Sci U S A 2009;106(8):2847–52. doi:10.1073/pnas.0812890106.
22. Hanahan D, Weinberg RA. Hallmarks of cancer: the next generation. Cell 2011;144(5):646–74. doi:10.1016/j.cell.2011.02.013.
23. Kircher MF, Hricak H, Larson SM. Molecular imaging for personalized cancer care. Mol Oncol 2012;6(2):182–95. doi:10.1016/j.molonc.2012.02.005.
24. Wahl RL. 2013 SNMMI Highlights Lecture: oncology. J Nucl Med 2013;54(11):11N–22N.
25. Rahmim A, Zaidi H. PET versus SPECT: strengths, limitations and challenges. Nucl Med Commun 2008;29(3):193–207. doi:10.1097/MNM.0b013e3282f3a515.
26. Rübe CE, Grudzenski S, Kühne M, Dong X, Rief N, Löbrich M, et al. DNA double-strand break repair of blood lymphocytes and normal tissues analysed in a preclinical mouse model: implications for radiosensitivity testing. Clin Cancer Res 2008;14(20):6546–55. doi:10.1158/1078-0432.CCR-07-5147.
27. Bourton EC, Plowman PN, Smith D, Arlett CF, Parris CN. Prolonged expression of the γ-H2AX DNA repair biomarker correlates with excess acute and chronic toxicity from radiotherapy treatment. Int J Cancer 2011;129(12):2928–34. doi:10.1002/ijc.25953.
28. Firsanov DV, Solovjeva LV, Svetlova MP. H2AX phosphorylation at the sites of DNA double-strand breaks in cultivated mammalian cells and tissues. Clin Epigenetics 2011;2(2):283–97. doi:10.1007/s13148-011-0044-4.
29. Wasco MJ, Pu RT. Utility of antiphosphorylated H2AX antibody (gamma-H2AX) in diagnosing metastatic renal cell carcinoma. Appl Immunohistochem Mol Morphol 2008;16(4):349–56. doi:10.1097/PAI.0b013e3181577993.

30. Podhorecka M, Skladanowski A, Bozko P. H2AX phosphorylation: its role in DNA damage response and cancer therapy. J Nucleic Acids 2010;2010. doi:10.4061/2010/920161
31. Djuzenova CS, Elsner I, Katzer A, Worschech E, Distel LV, Flentje M, et al. Radiosensitivity in breast cancer assessed by the histone γ-H2AX and 53BP1 foci. Radiat Oncol 2013;8:98. doi:10.1186/1748-717X-8-98.
32. Redon CE, Nakamura AJ, Martin OA, Parekh PR, Weyemi US, Bonner WM. Recent developments in the use of γ-H2AX as a quantitative DNA double-strand break biomarker. Aging 2011;3(2):168–74.
33. Lundholm L, Hååg P, Zong D, Juntti T, Mörk B, Lewensohn R, et al. Resistance to DNA-damaging treatment in non-small cell lung cancer tumor-initiating cells involves reduced DNA-PK/ATM activation and diminished cell cycle arrest. Cell Death Dis 2013;4:e478. doi:10.1038/cddis.2012.211.
34. Cornelissen B, Able S, Vallis KA. Targeting γH2AX during oncogenesis with Auger electron therapy delays tumor onset. J Nucl Med 2013;54(Suppl 2):121.
35. Cornelissen B, Waller A, Able S, Vallis KA. Molecular radiotherapy using cleavable radioimmunoconjugates that target EGFR and γH2AX. Mol Cancer Ther 2013;12(11):2472–82. doi:10.1158/1535-7163.MCT-13-0369.
36. Xie A, Puget N, Shim I, Odate S, Jarzyna I, Bassing CH, et al. Control of sister chromatid recombination by histone H2AX. Mol Cell 2004;16(6):1017–25. doi:10.1016/j.molcel.2004.12.007.
37. Celeste A, Difilippantonio S, Difilippantonio MJ, Fernandez-Capetillo O, Pilch DR, Sedelnikova OA, et al. H2AX haploinsufficiency modifies genomic stability and tumor susceptibility. Cell 2003;114(3):371–83.